J.P.J. Rinkel

The Formation of Wood Grains

A Model of Cell Growth
in the Vascular Cambium of Trees

Bachelor Thesis
January 5, 2015

Supervisor: Dr. R.M.H. Merks

Mathematical Institute, Leiden University

Contents

List of Figures

Supplemental Data

Supplementary Video S1 Rotation of cells in a growing meristem, as a result of mechanical stresses. Simulation as in Figure 4.6B.

Introduction

> When we no longer look at an organic being as a savage looks at a ship, as at something wholly beyond his comprehension (...) how far more interesting, I speak from experience, will the study of natural history become!
>
> - Charles Darwin, *On the Origin of Species*

> A fool sees not the same tree that a wise man sees.
>
> - William Blake, *The Marriage of Heaven and Hell*

This thesis is concerned with tree growth or, more specifically, the growth of tissues in the vascular cambium of trees. This might come as a surprise, as this thesis is presumed to be the closing chapter of a BSc degree in mathematics, whereas the chosen subject could be thought of to be more biological than mathematical. To think this, however, would be a flat mistake.
The use of mathematical techniques in biology is nowadays very common. Areas as different as calculus, probability theory, statistics, graph theory, dynamical systems, differential equations and, more surprisingly, even linear and abstract algebra, combinatorics, game theory and topology can be used to describe or explain a whole range of biological phenomena. Dynamical systems, for example, can be used to explain the growth of populations, while probability theory can describe aspects of genetic evolution.
The branch of game theory can be applied to investigate interactions between organisms and to explain which 'strategy' will be 'evolutionary stable'. For example, in sticklebacks (see Fig 1), two 'strategies' for selection of suitable mates by females are observed: choose or imitate. In the last case, a female selects the choice of another female. Now both strategies might be evolutionary stable, which means that an population in which this strategy is dominant, will not be invaded by another strategy. When the costs of choosing are higher then the benefits, a population of choosers is not unassailable and can be inflitrated by imitators, while this will not happen the other way around. This means that under these conditions, imitating will be a evolutionary stable strategy (Goldschmidt, 1994).
When these conditions change however, the stability of strategies also changes. This area of study is called 'evolutionary game theory'. Evolutionary game theory provides

Figure 1: *Gasterosteus aculeatus*, the three-spined stickleback. The female stickleback has several strategies for selection of a suitable mate. Evolutionary game theory is a branch of mathematics which studies the stability of these strategies. (Photo by Ron Offermans, Wikipedia Commons)

an even better application for game theory then the original economical one, as the last one assumes rational decision makers, while this is not necessary for the former (Maynard Smith, 1982).
These are examples of applications at the organizational level of (groups of) organisms, but besides that, mathematical biology can also be used at the lower level of the cell. Such a thing is done by using abstract algebra in genomics, a discipline of genetics. But mathematics can also be done in the field of 'systems biology', which is the same field that studies the growth of organ tissues. But before going on to the growth of plant tissues, it may be useful to take a broader look in the field of systems biology.
Traditionally, molecular biology has been primarily concerned with breaking organisms down to genes and proteins, and could be seen as a more reductionist, 'top down' approach to biology. Systems biology, at the other hand, tries to explain the workings of a biological system by looking at the interactions *between* these smallest fragments. In other words, systems biology is trying to "put Humpty Dumpty together again" (Noble, 2006).
Organs are such systems, and how organs develop (a process commonly named 'morphogenesis') is one of the central questions of systems biology. One of the first attempts to provide a mathematical model of this kind was undertaken by the well-known logician and computer science pioneer Alan Turing in his 1952 article 'A Chemical Basis of Morphogenesis' (Turing, 1952). Turing was interested in such things as the spots on butterfly wings and Dalmatian dogs, among others, and showed that chemical reactions could produce these patterns (Goodwin, 1994).
Another point of interest for Turing was 'phyllotaxis', the arrangement of the leaves in a plant. He was not the first to do so. Since the 19th century biologists and mathematicians have wanted to explain how the patterns in these arrangements (which show a relationship with the Fibonacci numbers) develop. In the field of developmental biology it is indeed one of the most striking examples of a process that can only be described by mathematical methods (Smith *et al.* , 2006).
The subject of this thesis, the formation of wood grains, is in a way a derivation of this problem. The wood grains mentioned here should not be confused with what is popularly called 'growth rings' or 'annual rings', the alternating rings of light and dark-coloured wood which can be observed in cut lumber. The wood grains we mean are a result of the fact that wood elements grow in elongated shapes, which are arranged

in parallel bundles (Kramer & Groves, 2003). These bundles are what we call 'wood grains'. These grains are mostly straight and parallel to the axis, but they might assume more complicated configurations, for example near branch junctions.
The growth of wood cells is regulated by growth hormones called auxins, which are distributed through the tissue by diffusion and active transport by PIN proteins. How the interaction between those chemicals influence the formation of wood grains is the subject of this thesis. A model to explain the formation of these patterns is given by Eric Kramer, who hypothesized that the fluxes of auxin, a growth hormone, in the cambium induce the cells to rotate (Kramer, 2002). In this thesis we will expand on his results. The questions we want to answer are: 1. How are auxin distribution and auxin flux orientation influenced by the cell form? and 2. How do auxin fluxes induce the cells to rotate or otherwise reorientate?
To do this we will use a computational method different from the one used in (Kramer, 2002). We will use VirtualLeaf, an open source framework developed by Roeland Merks and others, with the intent to model the growth and development of plant tissue (Merks *et al.* , 2011). VirtualLeaf uses a cell-based approach, which means it takes the cell and the processes in the cell to be the engine of morphogenesis, rather than the genome. We will use this approach to simulate the growth of and patterning of the so-called 'wood grains'.
But before we come to that, we will need a clear insight in the growth of trees and what we know of the formation of wood grains biologically. Besides that, we will consider already proposed mathematical models which have tried to explain this and related phenomena, like leaf venation.

Chapter 1

Pattern formation in trees

Before we are able to understand the model which will be proposed in this thesis, it is necessary to explain *how* a tree grows and what kind of patterns we mean by wood grains. This is what the first part of this chapter will be about. The second part will consider a model of pattern formation which was proposed earlier, and discuss its main results and shortcomings.

1.1 The vascular cambium and the development of wood grains

Growth and development of new wood cells occur only in the vascular cambium. When we think of the intersection of a tree branch *without* its bark, the vascular cambium will we the most outer region of what is left (Figure 1.1). The vascular cambium is a kind of secondary meristem, which means that it can produce daughter cells, which will differentiate in xylem and phloem cells. It typically is the only part of the branch were new cells form. The vascular cambium is only one cell thick and together with the adjacent layers of developing cells it is called the 'cambial region', which is in its totality 1 mm thick (Kramer, 2002).

The growth and subsequent division of cambial cells is induced by auxin, a phytohormone. There are many different types of auxin, of which indolent-3-acetic acid (IAA) is the most common and best-studied. Besides stimulating cell-growth, auxins play a mayor role in cell differentiation, growth of fruit and overall plant organization. Although auxin is of great importance in the development of trees, and plants in general, there are still a great many questions about it. One of the most significant ("Where is it produced?") is as yet not completely answered, although it is suspected that it is generated in the leaves of plants.

There are two ways in which hormones are transported through the cambium: diffusion, which is a result of different concentrations in adjacent cells; and active transport, which is caused by transport proteins in the cell. In the case of auxin, this second way of distributing auxin is known as 'polar auxin transport', which is characterized by the fact that it is directional.

For this kind of transport, PIN-proteins, among others, are responsible. Of this family, only the PIN1-protein is of interest here, because it appears to be the principal protein required for the development of new tissues (Jönsson *et al.* , 2006). Proteins of this type gather at cell membranes and stimulate the transport of auxin to bordering cells. It has been hypothesized that PIN1 transporters tend to localize to membranes neighboring

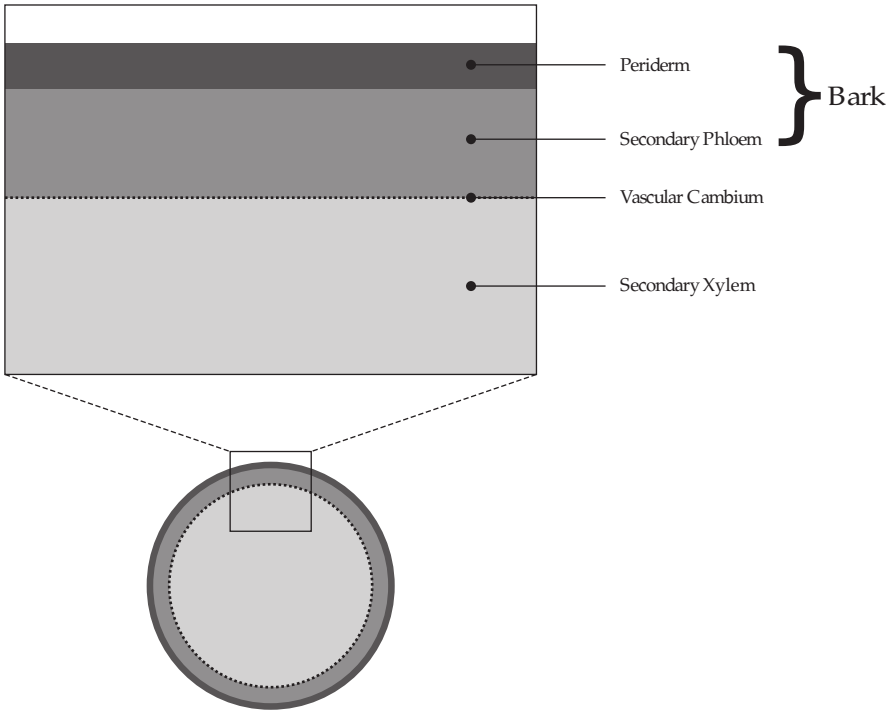

Figure 1.1: Cross section of a cut tree branch or stem, with the most important layers visible. 'Bark' is usually defined as "everything outside the vascular cambium", but in most cases, it contains the secondary phloem, the periderm and eventual dead tissues outside the periderm (Raven *et al.* , 1999).

cells with the highest auxin concentration (Jönsson *et al.* , 2006), thereby polarizing the auxin flux. This results in a feedback loop.

1.2 A mathematical model of pattern formation

As we mentioned earlier, mathematical models for pattern formation in the vascular cambium have already been proposed (Kramer, 2002), (Kramer & Groves, 2003). In it, he considers the cambium to be of negligible thickness, and calls it the *cambial surface*. Thus he creates a two-dimensional cambium. This cambium consists of fusiform initial cells, which rotate in the direction of the auxin flux, creating wood grains as a result. At the same time, auxin flows through the cells along their long axis.
Kramer defines $m(x, y, t)$ as the total mass of auxin at time t, averaged over a tangential area of 1 mm^2 in the neighbourhood of the point (x, y). The vector field $\mathbf{j}(x, y, t)$ signifies the auxin flux and includes the components $j_{||}$, which is the auxin flux measured parallel to the local grain direction and $j_\perp$ which is the auxin flux perpendicular to it. The grain direction $\mathbf{u}(x, y, t)$ is a unit vector tangent to the cambial surface, and $\mathbf{w}(x, y, t)$ is a vector field perpendicular to $\mathbf{u}$ (see also figure 1.2 for an illustration).
Defining $\nabla_\parallel m = \mathbf{u} \cdot \nabla m$ and $\nabla_\perp m = \mathbf{w} \cdot \nabla m$, Kramer finds for $j_{||}$ and $j_\perp$:

$$\begin{aligned} j_\parallel &= -D_\parallel \nabla_\parallel m + vm, \\ j_\perp &= -D_\perp \nabla_\perp, \end{aligned} \tag{1.1}$$

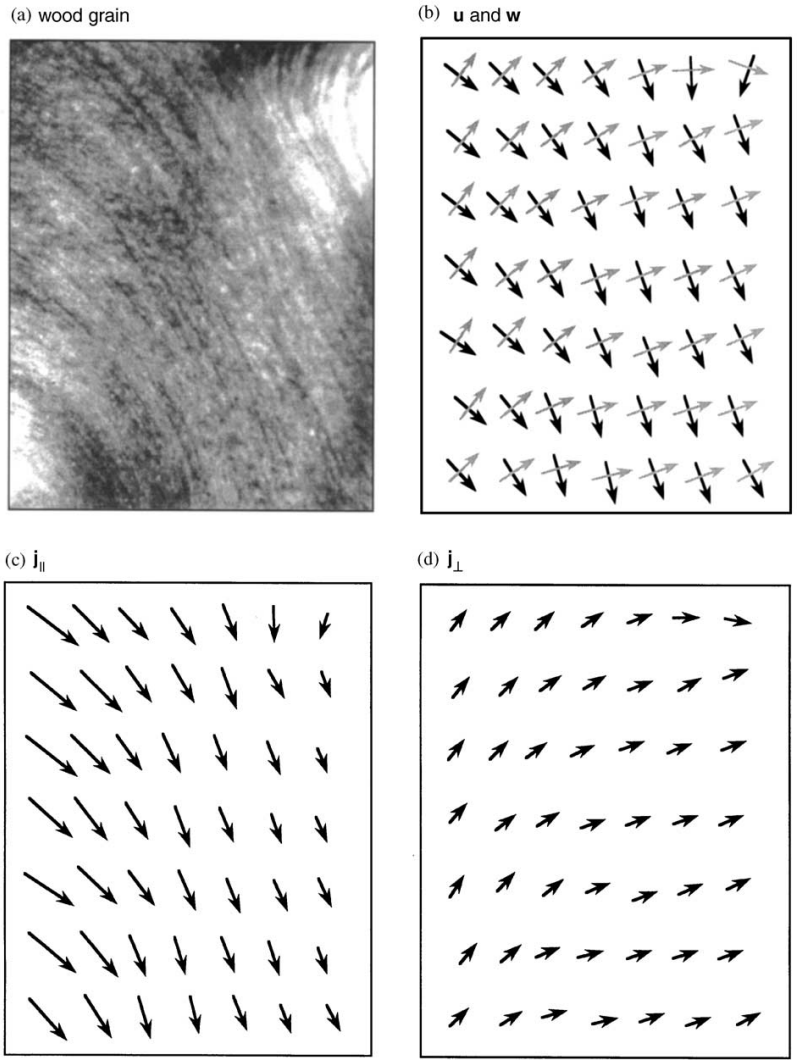

Figure 1.2: Illustration of the problem described by Kramer. (a) is a photograph of a debarked tree branch, with its wood grains clearly visible. (b) shows the vector fields **u**, which has the same direction of the wood grain, and **w**, which is defined as perpendicular to **u**. (c) and (d) show the auxin flux **j**, in which $j_{||}$ is the component oriented to the wood grain, which is mostly caused by active transport, while $j_{\perp}$ is the component perpendicular to it, which is mostly the result of outward diffusion. Taken from (Kramer, 2002)

in which $D_{\parallel}, D_{\perp}$ are constants of diffusion and v the velocity of auxin transport through the cambium. Because **j** is the vector sum of $j_{||}$ and $j_{\perp}$, it follows from equation 1.1 that for the total auxin flux **j** we have

$$\mathbf{j} = \left[-D_{\parallel}\nabla_{\parallel}m + vm\right]\mathbf{u} + \left[-D_{\perp}\nabla_{\perp}m\right]\mathbf{w} \tag{1.2}$$

For the auxin distribution $m(x, y, t)$ he gives

$$\frac{\partial m}{\partial t} = -\nabla \cdot \mathbf{j} = -\frac{\partial j_x}{\partial j_y} - \frac{\partial j_y}{\partial j_x}. \tag{1.3}$$

For the grain orientation, the angle field $\phi(x, y, t)$ is defined as $\phi = \tan^{-1}(u_y/u_x)$. From this, it follows that

$$\mathbf{u} = \cos(\phi)\mathbf{x} + \sin(\phi)\mathbf{y} \quad \text{and} \quad \mathbf{w} = -\sin(\phi)\mathbf{x} + \cos(\phi)\mathbf{y}. \tag{1.4}$$

It is now proposed that cells rotate to be in the same direction as the auxin flux. This rotation of the cell can be described by

$$\left.\frac{\partial \phi}{\partial t}\right|_{auxin} = -\mu \nabla_{\perp} m \tag{1.5}$$

in which μ denotes a proportionality constant. However, this results in very unrealistic patterns, containing very sharp kinks, the formation of which is irreversible (Kramer, 2002). So presumably something else is needed. In reality, cells excercise external stresses on each other by growing towards one another. This phenomenon is known as crowding. This was so far negated in this model, so this might explain the unrealistic events. Therefore the following equation is added, which describes this process as effective diffusion of cell orientations:

$$\left.\frac{\partial \phi}{\partial t}\right|_{crowding} = K \nabla^2 \phi \tag{1.6}$$

in which K represents a effective diffusion constant. Together, equations (1.5) and (1.6) lead to:

$$\frac{\partial \phi}{\partial t} = K \nabla^2 \phi - \mu \nabla_{\perp} m. \tag{1.7}$$

With equations (1.2), (1.3) and (1.7) we have a complete model for grain orientation and pattern formation.

1.3 Results for the model

Consideration is limited to static grain patterns. This means a time-independent version of the model is analyzed, i.e. the time derivatives are set to zero. For a more or less constant distribution of auxin, the equations are simplified to $\nabla \cdot \mathbf{u} = 0$ and $\nabla^2 \phi$ which are consistent with straight and spriral grains on cylindrical branches, or the circle patterns commonly found in whirled grain.
When the auxin distribution is varying, analytic solutions for m and ϕ are difficult or even impossible to obtain. Kramer uses numerical methods to examine several cases of pattern formation, by taking a square grid divided in smaller squares and defining a auxin source at the top and a auxin sink at the bottom. He then defines several defects on the grid.
As the first such defect, a hole is defined in the grid, which represents a wound or a knot in the vascular cambium. The hole is square shaped, and additional boundary conditions on the edge of the hole are given. For the vector normal to the edge of the hole $\mathbf{n}$, these conditions are defined $\mathbf{n} \cdot \mathbf{j} = 0$ and $\mathbf{n} \cdot \nabla \phi = 0$. The first condition ensures

that no auxin flows into the hole, while the second expresses that there is no preferred grain angle for cells adjacent to the edge of the hole. The result of the simulation is that the grains flow around the hole.
The second is like the first defect, with the difference that it has the shape of a diagonal slot. The result is also like the first, but it is noted that the grains have a strong tendency to align parallel with the long axis of the slot.
The result for the third defect is reproduced in Figure 1.3. In this figure, the white square designates a branch sticking out of the paper. The borders of the hole are made auxin sinks, with a flux comparable in magnitude to the flux on the upper boundary of the grid. Here the grain below the junction is directed downwards, while in the first defect it flowed around the edges of the hole. Lastly, the addition of topological defects, such as circle or X-patterns, which are often found in whirled grain, shows that these defects are stable.

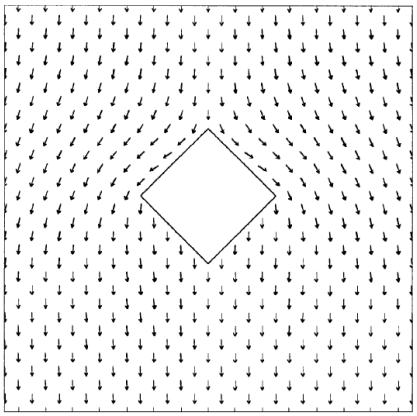

Figure 1.3: A result for the model described by equations (1.2), (1.3) and (1.7). This shows the grain direction surrounding a branch junction. Remark that the grains flow around the junction, but continue their way vertically to the bottom of the field. Taken from (Kramer, 2002).

The Kramer model has some notable aspects to it. First, there is the fact that in Kramers model cells rotate. As experiments have shown, cells in wood grain change orientation during their growth. But the growth of cells is never used in Kramers model, while this could explain the rotation. Cells might grow in another direction then along the original length axis, thereby changing the shape and consequently the orientation of the cells and the wood grains of which they are a part.
Another assumption made by Kramer is that the active transport of auxin flows perpendicular to the long axis of the cells, only to be (slightly) diverted by diffusion. But the means by which active transport is directed (i.e. PIN-transporters) is not mentioned, but this might be a very important feature of active transport. In the following chapter a model will be developed which includes those two aspects.

Chapter 2

A cell-based model of the vascular cambium

As we have seen in the previous chapter, the model proposed by Kramer inspires some follow-up questions. In this chapter, a new model will be introduced, which will hopefully do its work. This model is based on the model of Jönsson (Jönsson *et al.* , 2006), which was expanded by Merks (Merks *et al.* , 2007). In the first chapter, their work will be explained, while the second part is devoted to some, in this case necessary, adjustments to it.

2.1 A model for phyllotaxis

Because of the symmetries found in the involving patterns, the process of phyllotaxis, has experienced much interest by biologists. Many attempts have been made to explain the positioning of the leaves by mathematical models. One such model has been proposed by Jönsson (Jönsson *et al.* , 2006).
In this model, the concentration of auxin A is measured per cell i. The model takes into account both diffusion and active transport. Diffusion is dependent on the diffference between the concentrations of auxin in cell i and its neighboring cells j:

$$\left.\frac{dA_i}{dt}\right|_{diffusive} = T_{diffusive} \sum_j (A_j - A_i) \tag{2.1}$$

with $T_{diffusive}$ a constant. Active transport from cell i to cell j is dependent on P_{ij}, the amount of PIN1 in the membrane seperating i from j:

$$\left.\frac{dA_i}{dt}\right|_{active} = T_{active} \sum_j \left(\frac{P_{ji}A_j}{k_a + A_j} - \frac{P_{ij}A_i}{k_a + A_i} \right) \tag{2.2}$$

with T_{active} also a constant. Because active transport is presumed to have a significantly larger effect on the distribution of auxin, T_{active} is taken much larger than $T_{diffusive}$. k_a is a constant as well. This constant is a Michaelis-Menten constant, as the auxin distribution is regulated by a well-known but simple model of enzyme kinetics, called Michaelis-Menten kinetics (Michaelis & Menten, 1913).

Equations (2.1) and (2.2) together yield the complete equation for auxin distribution:

$$\frac{dA_i}{dt} = T_{active} \sum_j \left(\frac{P_{ji} A_j}{k_a + A_j} - \frac{P_{ij} A_i}{k_a + A_i} \right) + T_{diffusive} \sum_j (A_j - A_i). \tag{2.3}$$

Two equations regulate the distribution of the PIN-proteins:

$$\begin{aligned} \frac{dP_i}{dt} &= -k_1 \sum_j \frac{P_i(t) f(A_j(t))}{k_m + P_i(t)} + k_2 \sum_j P_{ij}(t) \\ \frac{dP_{ij}}{dt} &= k_1 \frac{P_i(t) f(A_j(t))}{k_m + P_i(t)} - k_2 P_{ij}(t) \end{aligned} \tag{2.4}$$

in which

$$f(A_j(t)) = \frac{A_j(t) R}{k_R + A_j(t)}. \tag{2.5}$$

In the these equations, k_m and k_R are Michaelis-Menten constants, while R is the total level of receptors. Together, the equations (2.3) and (2.4) constitute the complete model. One element that is not taken into account by Jönsson *et al.* is PIN-production and PIN-breakdown. Besides that, also the influence of the length of the cell membrane on diffusion is not reckoned with. But as these factors may contribute largely to the growth of cells in the vascular cambium, it might be needed to add them to the model. Proposals for such additions have been made, and we will see one in the next section.

2.2 A traveling-wave model

The Jönsson model has been expanded for the purpose of describing venation pettering in leafs own means (Merks *et al.* , 2007). Leaf venation is the result of cell differentiation. This last process is induced by auxin as well. To explain the patterning, the model is altered so that it uses the length of the cell membrane. Besides that, the production and breakdown of PIN-transporters is considered. The term describing diffusion is changed to

$$\left. \frac{dA_i}{dt} \right|_{diffusive} = T_{diffusive} \sum_j L_{ij} (A_j - A_i), \tag{2.6}$$

in which L_{ij} is the length of the cell membrane between cell i and neighbor j. Furthermore, the term $\alpha A_i - \delta P_i$ is added to dP_i/dt to include PIN-production of breakdown. But nor Jönssons model, nor these extensions to it, explain the formation of wood grain patterns. The new wood grain model is based on the Jönsson and Merks models, as will be described in the next section.

2.3 Description of the new meristem model

It is the objective here to develop a model in which the orientation of the auxin fluxes in elongated cells is properly described. According to exprimental date, the most auxin

is leaking from the short cell walls; 25% of the total amount of auxin is leaving the cell through the side walls, while the ratio between the long axis and the short axis is 20:1 (Mitchison, 1981). This is a significant difference and it might mean that PIN1-transporters tend to gather at the short cell walls.
It is possible to investigate elongated cells in our simulations, which provides us with the opportunity to make, in the new model, the distribution of PIN1 dependent on the length of the cell wall. The possible biological mechanism behind this will be further discussed in Chapter 5. Taking L_{ij} again as the length of the wall between cells i and j, equation (2.4) changes to

$$\begin{aligned} \frac{dP_i}{dt} &= -k_1 \sum_j \left[k_3 L_{ij}^a \cdot \frac{P_i(t) f(A_j(t))}{k_m + P_i(t)} \right] + k_2 \sum_j P_{ij}(t) + \alpha A_i - \delta P_i \\ \frac{dP_{ij}}{dt} &= k_1 \cdot k_3 L_{ij}^a \cdot \frac{P_i(t) f(A_j(t))}{k_m + P_i(t)} - k_2 P_{ij} \end{aligned} \tag{2.7}$$

in which we hold $f(A_j(t))$ to be equal to

$$f(A_j(t)) = \frac{A_j(t) R}{k_R + A_j(t)}. \tag{2.8}$$

The equation describing the auxin flux will remain unchanged:

$$\frac{dA_i}{dt} = T_{active} \sum_j \left(\frac{P_{ji} A_j}{k_a + A_j} - \frac{P_{ij} A_i}{k_a + A_i} \right) + T_{diffusive} \sum_j L_{ij}(A_j - A_i). \tag{2.9}$$

In equation 2.7 a, k_3 are constants. Suitable values for these parameters may be found by implementing the model in a computer simulation. This implementation will be the subject of the next chapter.

Chapter 3

Model implementation

THERE ARE NUMEROUS COMPUTATIONAL METHODS available to implement the model developed in the last section of the previous chapter. The open-source framework VirtualLeaf will be used to implement and analyse my model. In this chapter, we will try to explain what VirtualLeaf is and how it works. After that, we will describe how the model can be implemented in the framework.

3.1 Explanation of VirtualLeaf

The VirtualLeaf framework is developed to offer biologists ways to bring their hypotheses, which often consist of block-and-arrow diagrams, to life (Merks *et al.* , 2011). More systems like this have been developed before, but they require mathematical and computer programming skills, which many biologists do not have. VirtualLeaf is a modelling environment that needs only a little programming effort.

Cell growth

In VirtualLeaf cells are represented by polygonal finite elements, in which the edges of the polygons represent cell walls. Those cell walls are shared with adjacent cells, thereby restricting the relative movements of the cells. To describe cell behaviours like expansion and division, VirtualLeaf uses a Monte Carlo-based algorithm (Merks *et al.* , 2011). The algorithm is based on three simple rules:

1. The pressure of the turgor inside the cells exerts a uniform force on the cell walls.
2. The cell walls counteract the turgor pressure.
3. The walls expand when they are stretched, an expansion which is irreversible.

The relation between turgor pressure and cell wall resistance can be described in terms of a generalized potential energy (or Hamiltonian (H)):

$$H = \lambda_A \sum_i \left(a(i) - A_T(i)\right)^2 + \lambda_M \sum_j \left(l(j) - L_T(j)\right)^2 . \tag{3.1}$$

In this Hamiltonian we define a resting area $A_T(i)$ for cell i and a resting length $L_T(j)$ for cell wall j. These must be thought of as the areas and lengths cells and cell walls

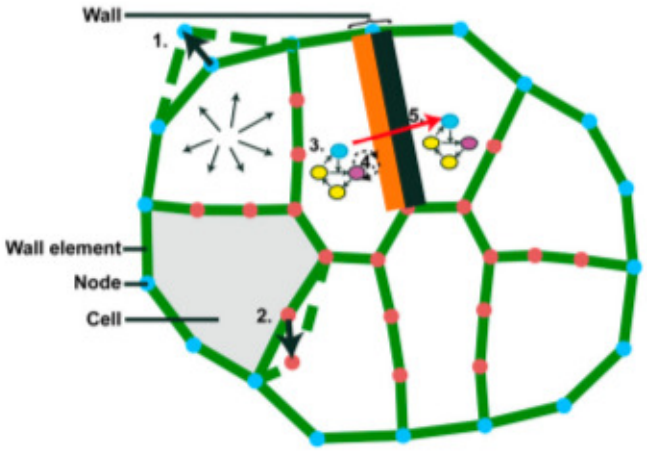

Figure 3.1: Illustration of the handling of cell growth by VirtualLeaf. Nodes of the cells-described-as-polygons are selected randomly and moved in a random direction. Moves are accepted if this results in a decrease of the potential energy. The result is an expansion of cell area and wall length. When the potential does not increase, the node will stay in its place. Taken from (Merks *et al.* , 2011).

assume when any turgor pressure is absent. Now a_i and l_j respectively are the actual cell area and wall length. The Hamiltonian sums over all the cells and the polygonal edges. λ_A is a parameter describing the cells resistance to compression or expansion and λ_M is a spring constant.
The algorithm now tries to minimize the potential energy H by selecting the nodes of the polygons randomly and moving it in a random direction. Whenever a certain move decreases the potential energy it is accepted, thereby increasing cell area and wall length. A potential move will be rejected when the potential energy would increase by accepting the move. See Figure 3.1 for an illustration. When the wall length is longer than a predefined value, new walls are made by adding nodes to the original wall, splitting the original wall in parts.

Cell elongation

For the implementation of my model, which needs cells to elongate, it is necessary to constrain the length of cells. This can be done by using the extended Hamiltonian H' (Merks *et al.* , 2011):

$$H' = H + \lambda_E \sum_j \left(e(j) - E(j)\right)^2 . \tag{3.2}$$

Here, $E(j)$ is the resting length of cell j, $e(j)$ the actual length of the cell and λ_E is a parameter giving the strength of the length constraint. In other words: a larger value for λ_E will induce cells to grow in a more elongated shape.

Cell division

Cell division is regulated by defining a division axis and building a new cell wall (consisting of several wall elements) along that axis. This way the original cell is split in two daughter cells sharing the new wall. Cell division is typically over the shortest axis,

which can be derived from the eigenvectors over the inertia tensor

$$I = \iint_D \begin{bmatrix} (x-x_c)^2 & -(x-x_c)(y-y_c) \\ -(y-y_c)(x-x_c) & (y-y_c)^2 \end{bmatrix} dx\,dy \tag{3.3}$$

Here, $\iint_D$ is the are integral over the cell and (x_c, y_c) is the cell's center of mass. The largest eigenvalue $\lambda_b(j)$ of I also serves to calculate the actual length of cell j, $e(j) = \sqrt{\lambda_b(j)/a(j)}$.

3.2 Implementing the meristem model

To obtain a meristem model in VirtualLeaf, we start by implementing a simple model, in which a bigger length constraint is used. By also restricting cell growth to the boundary cells of the stem, a vascular cambium is created. This method is a biomechanical one, in which the cells are forced to grow longer, independent from the auxin flux.
In Chapter 4, the results of this model will be used to obtain suitable parameters in my auxin-driven model. In the code for this model, two chemicals are defined, i.e. PIN1 and auxin. The individual cells have a colour depending on the concentrations of those chemicals; cells containing PIN will turn red, while cells containing auxin will turn green. The distribution of both PIN1 and auxin is regulated by the differential equations given in Section 2.3. Cells at the boundary may be defined as auxin sources, which means they produce auxin at a given rate.

3.3 The meristem vs. the cambial surface

Figure 3.2 shows the initial meristem we use to analyse the several instance of our meristem model. This does not represent the cambial surface, as was the case in (Kramer, 2002), but is a cross section of a stem or branch of a tree. This approach will somewhat limit the extent to which an effective comparison of our model to Kramer's can be made, but gives on the other hand a better means to analyse the growth of the cells and the effects of this on the auxin distribution. Consistent with this approach, cell growth will be restrained to the cells at the boundary of the meristem. Observe that the cells in the initial meristem are not yet elongated.

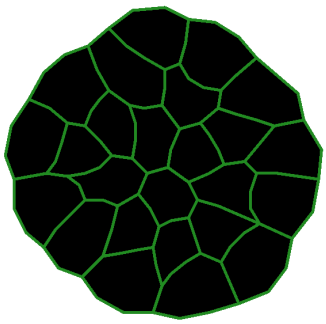

Figure 3.2: The initial meristem we use to analyse several instances of the meristem model.

3.4 Auxin orientation

In analyzing the results, we will consider what we will call the 'orientation' of the auxin flux, rather than the direction, as this last one might not be a good illustration of what is happening in a cell. For example, when a cell has the shape of a rectangle, with

comparable amounts of auxin leaving through the shorter edges, the direction of the auxin flux could be largely determined by the amounts of auxin leaving the long edges. The orientation of the auxin flux will be determinedy calculating the product of the normalvector of every wall with the ammount of auxin flowing through that wall. Every resulting vector with an vertical direction less then zero will be mirrored in the horizontal axis. This means that the orientation of every vector $[x, y]^T$ is to be determined using the atan2-function available in C++:

$$\begin{pmatrix} x \\ y \end{pmatrix} \mapsto \begin{cases} \begin{pmatrix} -x \\ -y \end{pmatrix} & \text{if } -\pi \leq \text{atan2}(y, x) \leq 0; \\ \begin{pmatrix} x \\ y \end{pmatrix} & \text{otherwise.} \end{cases}$$

Summing over all the wall elements will result in the required orientation.

Chapter 4

Results

As explained in the previous chapter, we will run a very simple model to begin with, thereby setting an example for the auxin-driven model. When suitable parameters for this model are found, the creation of disturbances in the vascular cambium will be examined.

4.1 Model dynamics

We consider a simple configuration, with three cells 1, 2 and 3, with cell 1 and 3 bordering cell 2, without bordering each other (see Figure 4.1 for an illustration). We take A_i, P_i as resp. the auxin concentration and the PIN1-concentration for cell i. We denote the concentration of PIN1 in the membrane of cell 1 and 3 adjacent to cell 2 as Pw_1, Pw_3 and for the membranes of cell 2 adjacent to cell 1 and 3 we take Pw_{2L} and Pw_{2R} respectively. The length of the wall between cell 1 and 2 is equal to L_1, while the length of the wall between cell 2 and 3 is equal to L_3.

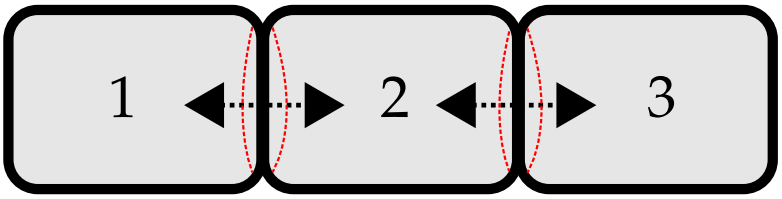

Figure 4.1: A simple configuration with three cells. Auxin flows between cell 1 and 2, and cell 2 and 3. PIN1 stays in the cells and flows from the inner cells to the membranes, which are depicted by the red dashed lines.

We assume that no auxin is produced nor broken down, so $A_1 + A_2 + A_3 = 1$. Furthermore, we assume that the total PIN1-concentration in every cell is constant, yielding the equation $P_1 + Pw_1 = P_2 + Pw_{2L} + Pw_{2R} = P_3 + Pw_3 = 1$. For the PIN distribution we consider the system

$$\begin{aligned}
\frac{dP_1}{dt} &= -k_1 k_3 L_1^a \cdot \frac{P_1 f(A_2)}{k_m + P_1} + k_2 Pw_1, \\
\frac{dP_2}{dt} &= -k_1 k_3 \frac{P_2}{k_m + P_2}\Big[L_1^a f(A_1) + L_3^a f(A_3)\Big] + k_2\Big[Pw_{2L} + Pw_{2R}\Big], \\
\frac{dP_3}{dt} &= -k_1 k_3 L_3^a \cdot \frac{P_3 f(A_2)}{k_m + P_3} + k_2 Pw_3,
\end{aligned} \tag{4.1}$$

with

$$f(A_j) = \frac{A_j R}{k_R + A_j}. \tag{4.2}$$

Like Jönsson, we assume that the PIN polarity is in quasi steady state (Jönsson *et al.* , 2006). Because we may as well assume that most PIN1 gathers at the membranes (so $k_m >> 1$), we take $\frac{P_i}{k_m+P_i} \approx \frac{P_i}{k_m}$. In this case, the system has equillibria

$$\begin{aligned} Pw_1^*(A_2) &= \frac{k_m k_1 k_3 L_1^a}{k_1 k_3 L_1^a f(A_2) + k_2 k_m}, \\ Pw_{2L}^*(A_1) &= \frac{k_m k_1 k_3 L_1^a}{k_1 k_3 L_1^a f(A_1) + k_2 k_m}, \\ Pw_{2R}^*(A_3) &= \frac{k_m k_1 k_3 L_3^a}{k_1 k_3 L_3^a f(A_3) + k_2 k_m}, \\ Pw_3^*(A_2) &= \frac{k_m k_1 k_3 L_3^a}{k_1 k_3 L_3^a f(A_2) + k_2 k_m}, \end{aligned} \tag{4.3}$$

Because $A_2 = 1 - A_1 - A_3$ the equillibria can be expressed solely as functions of A_1 and A_3. For $A_1,\ A_3$ we have the system

$$\begin{aligned} \frac{dA_1}{dt} &= T_{active}\left(\frac{Pw_{2L}A_2}{k_a + A_2} - \frac{Pw_1 A_1}{k_a + A_1}\right) + T_{diffusive}L_1(A_2 - A_1), \\ \frac{dA_3}{dt} &= T_{active}\left(\frac{Pw_{2R}A_2}{k_a + A_2} - \frac{Pw_3 A_3}{k_a + A_3}\right) + T_{diffusive}L_3(A_2 - A_3). \end{aligned} \tag{4.4}$$

The equilibria of this system given in (4.4) are can not be determined explicitly, but the Jacobian matrix of the system is equal to

$$DF = \begin{pmatrix} -T_{active}Pw_1 - T_{diffusive}L_1 & 0 \\ 0 & -T_{active}Pw_1 - T_{diffusive}L_3 \end{pmatrix} \tag{4.5}$$

This has for all A_1, A_3 the eigenvalues

$$\lambda_1 = -T_{active}Pw_1 - T_{diffusive}L_1,\ \lambda_2 = -T_{active}Pw_1 - T_{diffusive}L_3.$$

So all equilibria of the system (4.4) are stable.

4.2 Numerical analysis

It is difficult to determine the equillibria of the system described in (4.4) algebraicly, but it is possible to do this numerically. This also gives a method to investigate our model for several values of a. Reasonable of values for some of the other parameters have already been determined (Merks *et al.* , 2011), so we will use these values for convenience here and only vary k_3 and a.
Using a MATLAB script in which a Forward Euler method (with time step $h = 0.1$)

was implemented. We evaluated the system for several sets of initial values. The results are given in Figure 4.2. Here we have defined parameters $k_1 = 2 \times 10^{-4}, k_2 = 5 \times 10^{-7}$ and $k_m = 100$, $k_a = 1$ and $K_r = 1$, while $T_{active} = 0.06$ and $T_{diffusive} = 1 \times 10^{-6}$.

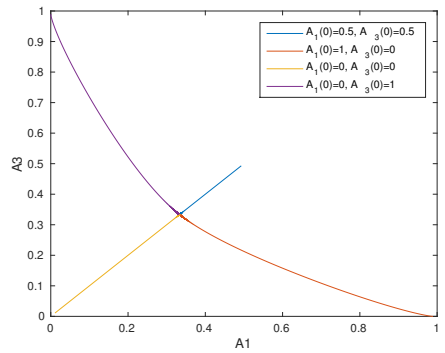

(a) $a = 1$, with equal wall lengths

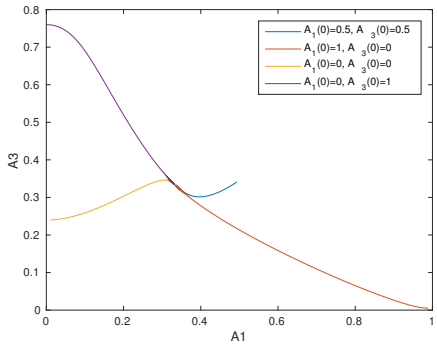

(b) $a = 1$, with $L_1 = 1$, $L_3 = 20$

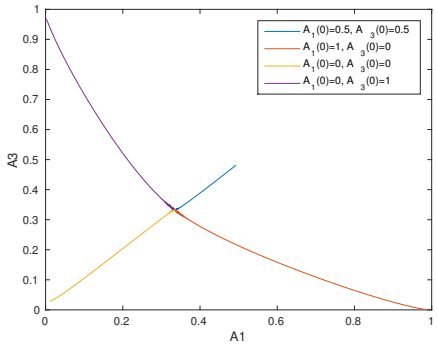

(c) $a = 0.3$, with $L_1 = 1$, $L_3 = 20$

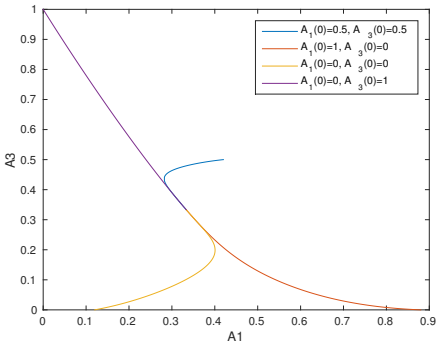

(d) $a = -2.5$, with $L_1 = 1$, $L_3 = 20$

Figure 4.2: Numerical results for the simplified model defined by equations (4.3) and (4.4), for several values of a and different wall lengths L_1 and L_3. All results are given after 20.000 time steps (besides **(d)**, which is given after 100.000) and for $k_3 = 1$ (again besides **(d)**, which has $k_3 = 10$).

Figure 4.2a presents the ordinary case, with $a = 1$ and $k_3 = 1$, for comparison. We see that for every initial condition, the system converges almost linearly to $A_1 = A_2 = A_3 = \frac{1}{3}$. The next step is varying the wall lengts. For the new wall lengths, we take the values mentioned in Section 2.3, which gives us $L_1 = 1$ and $L_3 = 20$. Figure 4.2b shows the results for this new configuration under the ordinary values for a and k_3. We see that the system still converges to the same values, but it can also be observed that there is a slight preference for cell 3, which is apparent from the steeper slope of the yellow line.
To induce a preference for the short cell walls, we need a value of $a < 1$, with $a \neq 0$. A result for $0 < a < 1$ is given in 4.2c, which shows that this will only reverse the increased preference for the longer cell walls. Choosing a value of $a < 0$ does increase the preference of auxin for the shorter cell walls, which is shown in 4.2d. However changing the value of a does not change the steady state of the model.
We conclude that negative values of a will give us favorable results. From simulations with several values of k_3 we see that lower values result in a higher preference for the short walls.

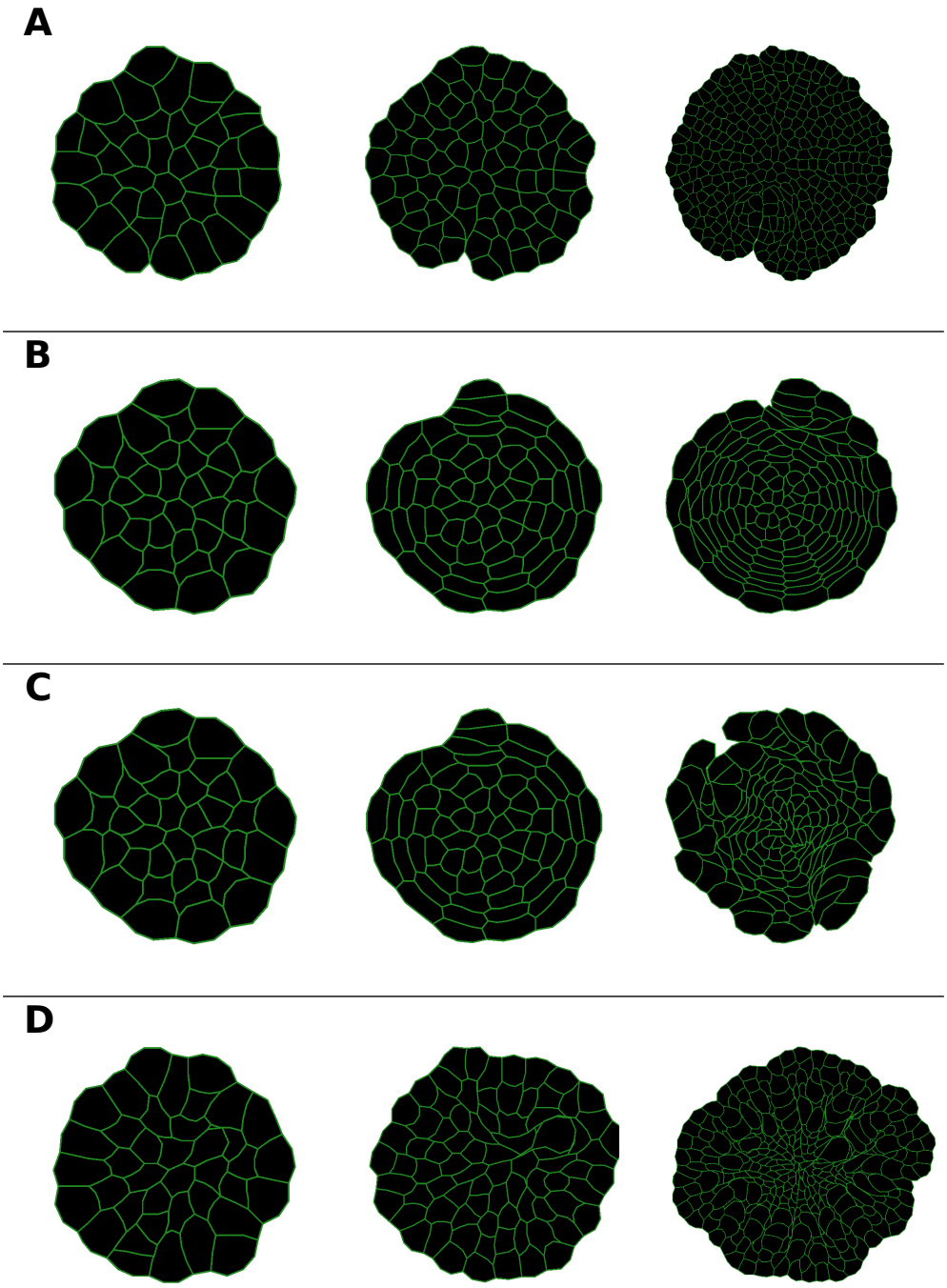

Figure 4.3: Illustration of three stages (after respectively 500, 1000 and 3000 time steps) of the biomechanical model, for several parameter configurations. A, $\lambda_E = 0$, so no cell elongation occurs. B, cell elongation is restricted to the boundary cells $\lambda_{E_{boundary}} = 12$. In C, cell elongation is extended to the internal cells as well with cells elongating stronger at the boundary, with $\lambda_{E_{internal}} = 8$ and $\lambda_{E_{boundary}} = 12$. D has $\lambda_{E_{internal}} = 12$ and $\lambda_{E_{boundary}} = 0$.

4.3 A biomechanical model of wood meristem

The elongation of cells is regulated by a parameter λ_E (see Section 3.1). Also, we are able to differentiate between several types of cells (i.e. boundary and internal cells) and vary the value of λ_E for each different type. In Figure 4.3 on page 22 the results for several combinations of parameters are given. For a good comparison of the effects of changing λ_E, example A shows a result when $\lambda_E = 0$ in all cells. We see that the shapes of the new cells are like round blots. This changes when we allow the boundary cells to elongate. For $\lambda_{E_{boundary}} = 12$ we see thin, circular patterns emerge (B). This image conforms with what we know of the way a branch grows.
The other figures show less realistic patterns. C has the internal cells elongating as well. $\lambda_E = 8$, so the internal cells are less inclined to grow longer. Although growth is disabled for the the internal cells forces excercised on them by the outer cells squeeze them together, something which does not happen in B at all. Reversing the roles gives us another remarkable result. When elongating in the boundary cells is disabled (D) we see that the meristem consists of three layers: the centre, containing only small cells, squeezed together; a ring in the middle, containing larger cells; and a boundary, containing the blot-shaped cells we already encountered in A.
The last two instances only serves to investigate the effects of several values for λ_E as B already gave us a workable example.

4.4 Simulations with static tissue

Simulations of feedback with auxin flux and tissue geometry in static tissue may provide more insight in the behaviour of the model for different combinations of parameters. Figure 4.4 on page 24 shows the results for several values of a and k_3. For a good comparison, the first instance (A) uses values $a = 0$ and $k_3 = 1$, thus effectively recreating the original travelling-wave model described in the beginning of Chapter 2. According to the values found in the previous section, $a = 0.35$ was used in the second example (B).
The results are represented in several ways. Here, the first three pictures of every column show the transporters between all the cells after several time steps. The purple borders depict auxin sources. The reason for this, is that auxin is assumed to be produced at the tips of branches for the cells, and distributed at the barks of the trees. The transporters colouring red are filled with PIN1-proteins. The fourth picture shows the cells. As was mentioned before, cells containing PINs are coloured red and those containing auxin green. The white bars represent the orientation of the resulting auxin fluxes (see Section 3.4).
The simulation shown in Figure 4.4B gives some more results. The first one is that the PINs are more inclined to gather at the short walls of the cells, than they do in the variant without any specified preference. Secondly, it is mainly in the boundary cells that they concentrate in the membranes, which is a consequence of the presence of auxin in those cells. Thirdly, the auxin fluxes are mostly oriented along the long axes of the cells. A negative result is the yellow-coloured cell, which indicate a large concentration of both auxin and PIN1, while some cells are still coloured black, and there is almost no auxin in the boundary cells.
To further investigate the effects of cell wall preference, another simulation (C) has the PIN's preference for shorter walls made stronger by setting $a = -2.5$. This resulted in

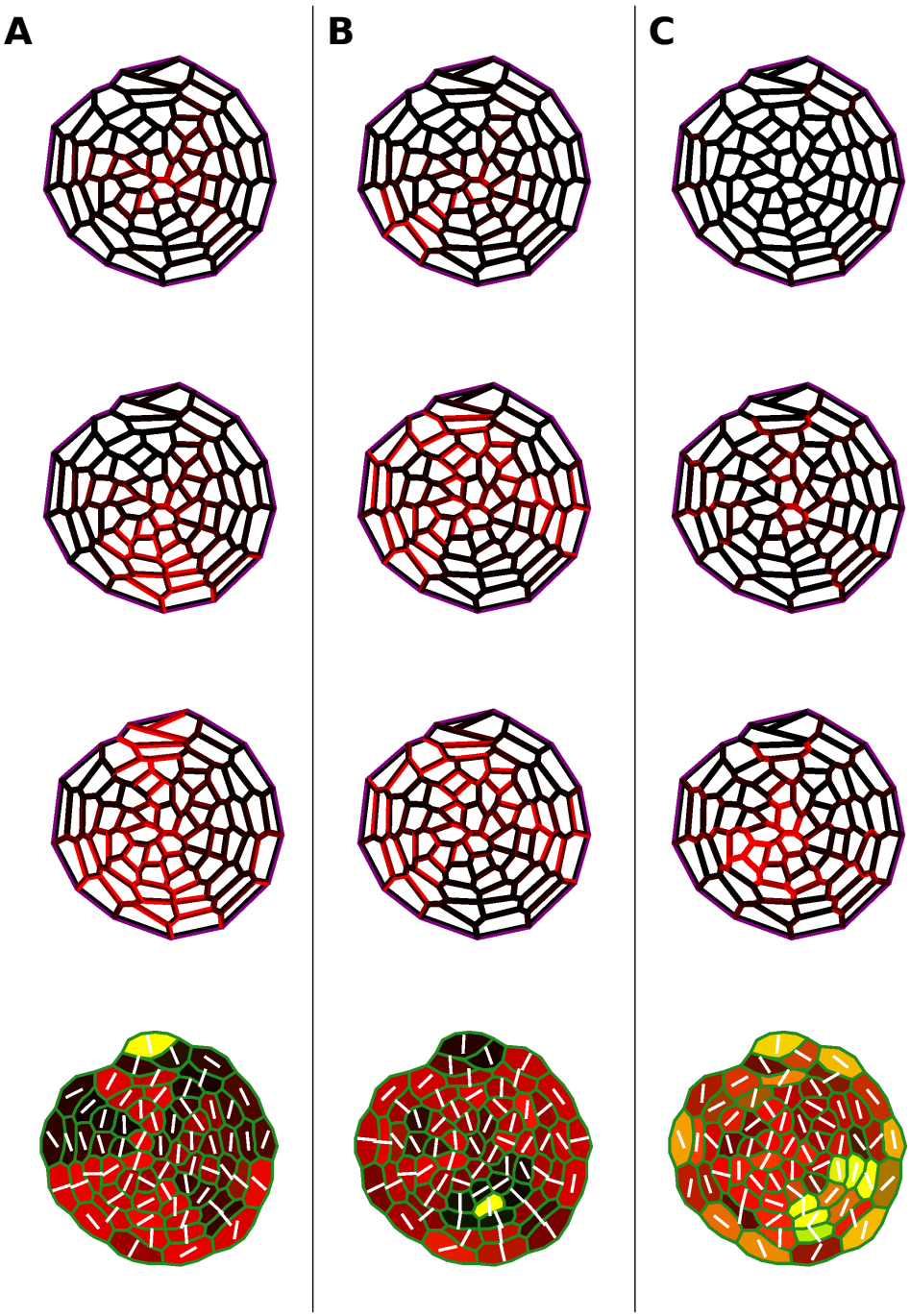

Figure 4.4: The stages of three simulations with static tissue. *A*, the "normal" variant, with $k_3 = 1$ and $a = 0$. *B*, $k_3 = 1$ and $a = 0.35$. *C*, $k_3 = 10$ and $a = -2.5$. From all three simulations the transporters are shown after 100, 250 and 500 time steps, and the cells after 500 time steps. *Purple* cell wands indicate auxin sources; *red* ones indicate that the transporter is filled with PIN1. In the fourth row, *red* depicts a cell filled with PIN1 and *green* cells contain auxin. The white bars represent the orientation of the auxin flux (see Section 3.4)

a slower circulation of the PIN-proteins, which can also be inferred from the model description, as L_{ij}^{a} will be smaller for smaller (negative) values of a. Like in Section 4.2, we set k_3 equal to 10. The results are shown in Figure 4.4C. As expected, the shorter walls colour red faster, which also results in the preferred orientation of the PINs. Another positive feature of this simulation is that the auxin is more evenly distributed, which results in a larger amount of auxin in the boundary cells.

4.5 Growing tissue

The previous section showed the effect of different parameters on the distribution of PINs and auxin. Now it is time to take the model a step further by introducing tissue growth.

Tissue growth

To regulate tissue growth, we introduce a few rules. One: we only allow boundary cells to grow; and two: we define a treshold τ for the amount of auxin needed to stimulate growth. These rules were implemented in the VirtualLeaf model. As the set of parameters $k_3 = 10$ and $a = -2.5$ proved to be the most satisfactory combination, this was together with an threshold of $\tau = 2.5$. This value was based on the amounts of auxin present in the boundary cells at the latter states of the simulations described in the previous chapter.

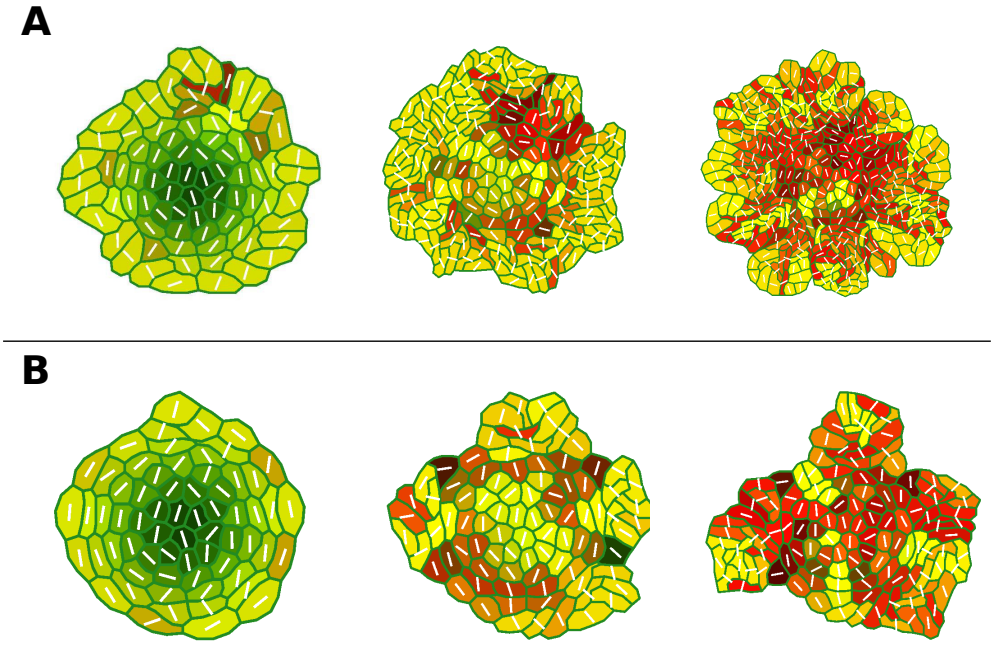

Figure 4.5: The states of three simulations with growing tissue. All three of them use $k_3 = 10$ and $a = -2.5$. *A*: Simulation states for threshold $\tau = 2.5$. *B*: Here, the threshold is raised to $\tau = 7$, as a mean to limit the growth rate. For both simulations the cells are shown after 100, 250 and 500 time steps.

The morphologies following from these assumptions are shown in Figure 4.5A. What we see is some very 'tumour-like' growth and the speed with which it grows is very high.

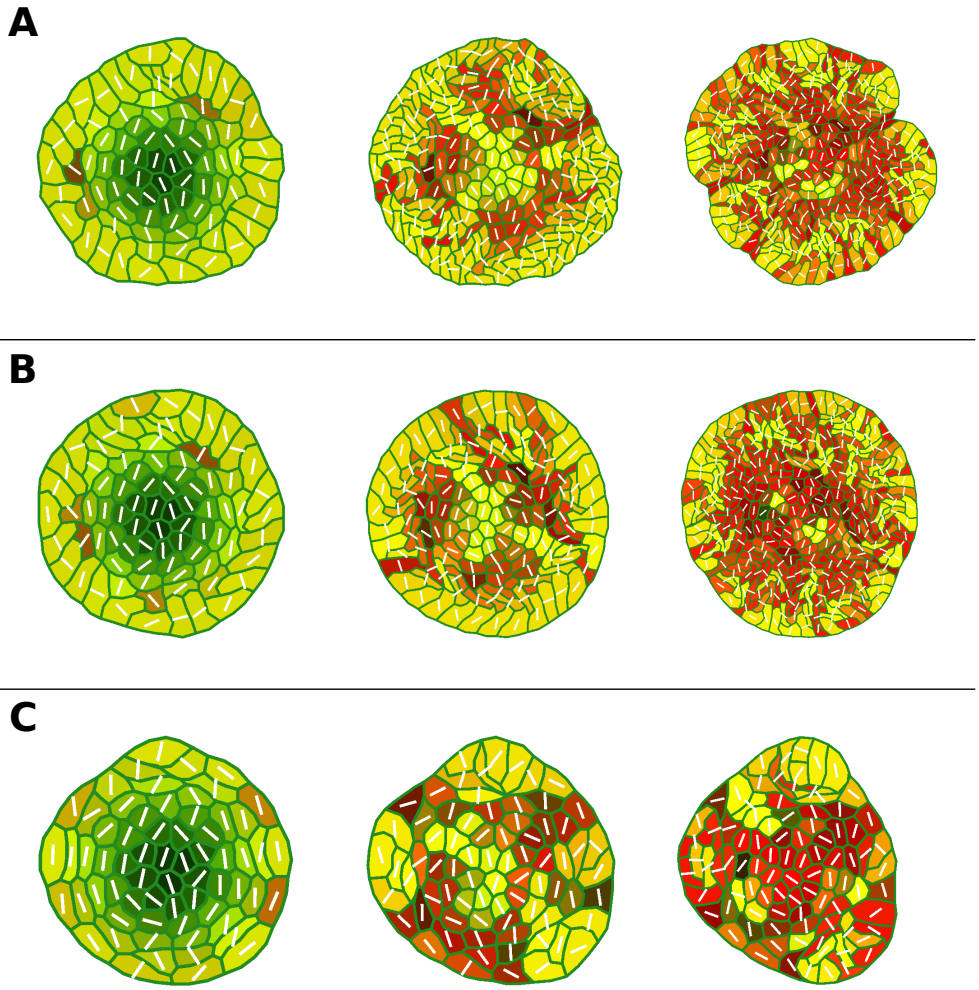

Figure 4.6: To constrain the tumorous growth encountered in the first two simulations, the relative perimeter stiffness (see page 26) is set set to different values. A, $\zeta = 4$; B, $\zeta = 7$; and C, $\zeta = 8$. For all three simulations the cells are shown after 100, 250 and 500 time steps. NOTE: For regularity's sake, $\zeta = 6$ was tried as well, instead of $\zeta = 7$. Unfortunately, VirtualLeaf was not able to reach the 500 time steps for this parameter, a subject which will be touched upon in the next chapter.

This is accounted for by the fact that auxin concentrations seem to raise higher then was induced by the results in Section 4.4. Raising the threshold to $\tau = 7$, results in the simulation shown in Figure 4.5B. While this simulation shows a more moderate growth rate, it nevertheless fails to constrain the tumorous growth we already encountered in the first example.

Perimeter stiffness

A way to reduce the tumorous growth, is to look at the 'relative perimeter stiffness'. If we define λ_m(wall) as the stiffness of a wall, we may also say that λ_m(perimeter) = $\zeta\lambda_m$(internal), for some ζ. As cell walls tend to be thicker and stiffer at the perimeter, it is assumed that $\zeta = 2$ in leaf morphogenesis (Merks *et al.* , 2011). But it is thinkable that the relative perimeter stiffness of wood cells is even higher. This gives us a new possible way to create a model which describes the formation of wood grains. Figure

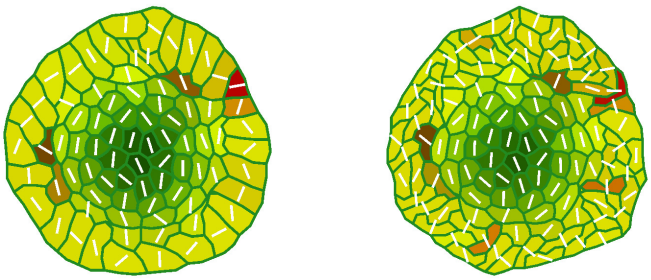

Figure 4.7: Model B after resp. 109 and 115 time steps. Observe how different the patterns have become in a very short time. See also Supplemental Video S1.

4.6 gives the results for three different values of ζ.
We see that for $\zeta = 4$ (A), the model gives us good results at the beginning, but when it runs longer, it starts to develop 'bumps' in the boundary. The result for $\zeta = 7$ (B) resembles the growth of a meristem. The external shape of the result stays much like a 'round' stem or branch. Both A and B show a remarkable aspect, because at certain times, mostly while the boundary cells divide, the cells all seem to turn around and realign.
Figure 4.7 shows two results of the simulation in Figure 4.6B, after 109 and 115 time steps respectively. We may observe that in a very short time the patterns have changed almost completely (see also Supplemental Video S1 for a clearer perception). This brings Kramer's rotating cells back to mind (see equation (1.5)). However, here the rotations occur only as a consequence of mechanical stresses exercised upon them, i.e. the cells don't rotate by themselves. Besides that, the rotations occur completely independent from the auxin flux. They don't orient along the auxin flux.
The simulation using $\zeta = 8$ (C) shows us a very slowly growing meristem. Here the relative perimeter stiffness is clearly to big to allow the cells to grow.
Overall, enabling cell growth gives results which show some resemblance to some of the results in by Kramer (Kramer, 2002). This is best seen in Figure 4.6B, and in the initial stage in Figure 4.5B.

4.6 PIN polarity vs. cell geometry

The cells in the preceding simulations grow in an elongated shape. This is a result from the elongated shape of the boundary cells in the initial leaves, which is inherited by the daughter cells. The idea is now to investigate what will happen when we: 1. Disable the elongation of the cells; and 2. Permit the elongation, but disable the preference of the PIN1 for the shorter cell walls. Simulations with this objective are given in Figure 4.8.
In Figure 4.8A, we start with a new leaf which has grown from the leaf shown in Figure 3.2, but which consists solely of rounded cells instead of elongated ones. On this we used the meristem model developed in Chapter 2, with $a = -2.5$ and $k_3 = 10$. Growth only occurs in the boundary cells when the concentration of auxin is higer than the threshold $\tau = 4$. We observe that growth occurs here, but of only slightly elongated cells, in which the PIN-orientation is parallel to the boundary of the meristem.

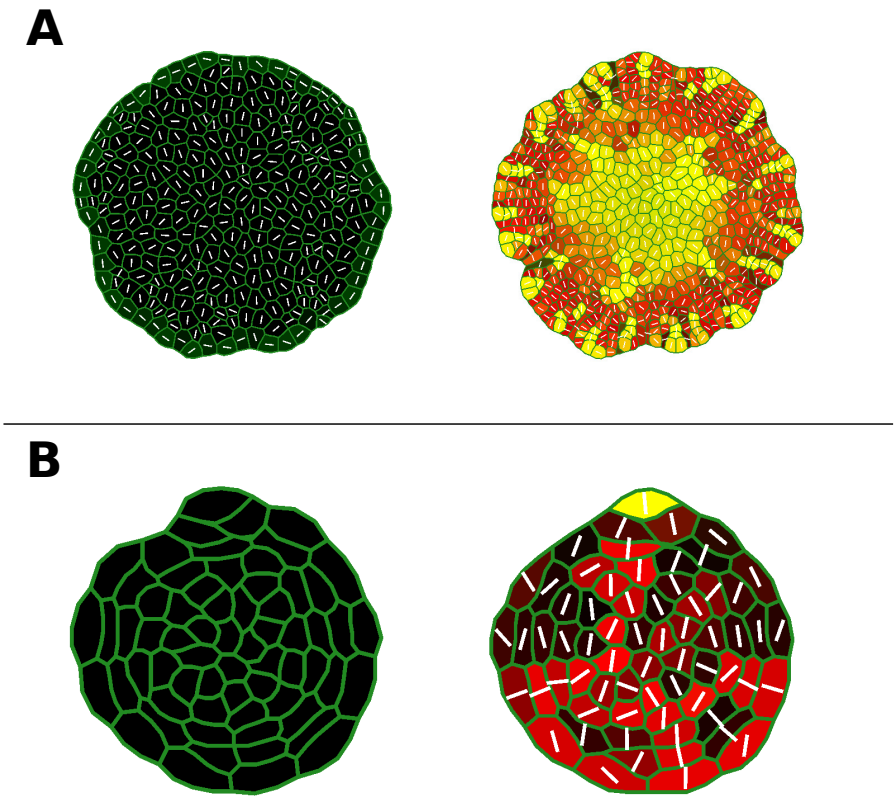

Figure 4.8: Simulations with cell elongation disabled (A) and with cell elongation, but without the preference of PIN1 for shorter walls (B). For both simulations the initial leaf and the result after 450 time steps are shown. We observe that in A the cells grow in only slightly elongated shapes, while in B there is almost no growth at all, as all auxin flows to the center of the leave. Comparing this with Figure 4.6B let us conclude that PIN-orientation and the geometry of the cell strengthen each other.

In Figure 4.8B we have used the same initial leaf which was also used in the simulations in Figures 4.4, 4.5 and 4.6, but this time the PIN1 follow the model in (Merks *et al.* , 2011). This results in almost no growth at all, because the auxin leaks through the longer cell walls and ends up in the center of the meristem. This means that the threshold of $\tau = 4$ is not reached. Simulations with lower threshold values gives similar results.
When we compare these results to that of Figure 4.6B, we may conclude that the polarity of the PIN1 and the elongated growth strongly influence each other. Indeed, without the preference of PIN1 for the short walls, almost no growth will even occur in the meristem, while the result in 4.8A shows that this preference may induce a slight elongation of new cells. However, as is seen in Figure 4.6B, it helps a great deal if the initial leaf already has some elongated cells.

Chapter 5

Discussion

The research questions for this thesis are: 1. How does the form of the cells influence auxin distribution and flux orientation? and 2. How do auxin fluxes induce the cells to orient? With the results in Chapter 4 it is possible to give a preliminary answer to those questions.

5.1 Conclusions

Kramer observed that in wood grains, auxin tends to follow the shape of the elongated cells, but also that these auxin fluxes are parallel to the boundaries of the tissue examined (Kramer, 2002). The first phenomenon resulted in auxin flowing primarily through the short cell walls. The model described in Section 2.3 reproduces these results. For example, an evaluation of the ODEs for a simple configuration shows that, when there is only auxin in the middle cell, it will initially flow to the adjacent cell which has a shorter common border. This is also observed in Figure 4.4. This figure also reproduces the same auxin flux orientation for border cells. This means that at least for static tissue, the proposed model gives an explanation for the orientation of the auxin fluxes; the simulations show us that the concentration of PIN1-molecules at the short edges of the cell might be causing this to happen.
As to the underlying biological process, it is probable that microtubules, the components of the cytoskeleton of the cells, help to explain the hypothetical inclination for PINs to the shorter cell walls. Some research suggest a connection between the orientation of the microtubules and the polarity of the PIN1-proteins and a relation between the shape of a cell and the formation of the cytoskeleton (Heisler *et al.* , 2010). At the other hand, this research also supposes it to be more likely that the microtubules are orientated the other way around, thereby sending the PINs to longer walls rather than the short walls. But it is nevertheless possible that this works the other way around in wood cells, so here further research is also needed.
An answer to the second question is also partially given by the simulations. In Figure 4.8 it is observed that cells grow elongate slightly and orient parallel to the boundaries of the meristem when the distribution of auxin is prescribed by the in this thesis developed model. When this preference for short cell walls is lifted, almost no growth occurs at all. As the proposed model states no relation between cell growth and auxin orientation, the orientation of the cells is only a result of mechanical stresses. However, the alignment of the cells is noticed more strongly when the initial meristem contains already some elongated cells. This means that adaptations of the model in which the auxin flux

orientation may cause the cells to grow longer must be the subject of further research.

Further research

As a link between auxin flux orientation and the orientation of the cell growth might be the object of further research, two directions for establishing such a link might be thought of.

1. *Adapting the direction of cell growth.* Making the direction of the cell growth dependent on the auxin concentration could induce cell elongation. Biologically this could be seen as auxin 'pushing' the cell wands forward. However, the existence of such a mechanism in nature is at this point hypothetical, altough some research suggests at least a role this for auxin (Zaban *et al.* , 2014).
   In terms of VirtualLeaf, this would mean that nodes whith a higher nearby concentration have a higher chance of being chosen first by the algorithm. The chance for each node to be chosen would then depend on the concentration of auxin in the adjacent cell walls.

2. *Altering the direction of cell division.* Another way of forcing the cells to elongate is to force cells to divide along the ax which is parallel to the auxin flux. As auxin is directed at the shorter walls, dividing along this axis would mean the daughter cells will almost always be longer than their parents. Biological research suggest that such a link between auxin and cell division might exist (Yoshida *et al.* , 2014). As VirtualLeaf allows us to choose the axis of division, such an adaptation might not be hard to implement.

With a model which incorporates one of these (or even another) adaptations, one could investigate if the auxin flux is really able to induce the wood cells to align and form wood grains. In Section 4 it was explained that we attempted to simulate the growth of a cross section of the stem or a branch of a tree. In this perspective, an useful result from (Kramer, 2002) is given in Figure 1.3.
In it, the wood cells inside the square are not shown, but they must indeed be there and they must be of the form of a meristem, as the square might be seen as a cross section of a branch as well. This means a readjustment of our model in which the cells on the top of the meristeme stay auxin sources, while the cells at the bottom are defined as auxin sinks should form something which might take the place of the square in Figure 1.3. One does not need much fantasy to fill in the grains in this figure, so a comparison between the results in VirtualLeaf and the result of Kramer can easily be made.
Finally, one last remark must be made concering further research: the huge concentrations of auxin and PIN1 are of dimensions which seem not actually possible, so maybe the production of both auxin and PIN1 might be regulated, for instance by applying some Michaelis-Menten kinetics (Michaelis & Menten, 1913). But, as the simulations are run on a cut branch of a plane, the efflux of auxin, which is not taken into account in the simulations done in this thesis, might be simulated by adding the breakdown of auxin.

5.2 Possible improvements concering VirtualLeaf

VirtualLeaf provides a handy tool to investigate the interaction of different types of chemicals and their influence one cell growth. It nevertheless has its limitations, which defines the limits of this project as well:

- It was not possible to check whether the ratio between the amounts of auxin leaking through the shorter walls vs. the amounts leaking through the longer ones was equal to the established ratio of 25:75.
- Several attempts were made at creating a single-cell model in VirtualLeaf, constructing or drawing a cell with suitable dimensions was not feasible. The same problem arose when creating the initial leaf which I used in all of my simulations. Any future update of VirtualLeaf featuring some kind of editor would be a huge improvement.
- VirtualLeaf uses an adaptive-step-size Runge-Kutta algorithm, which causes the software to terminate now and again. This is a result of the fact that auxin concentrations raise to high for the algorithm to adapt to.

References

Goldschmidt, Tijs. 1994. *Darwins hofvijfer.* Amsterdam: Uitgeverij Bert Bakker.

Goodwin, Brian. 1994. *How the leopard changed its spots.* London: Weidenfeld & Nicolson.

Heisler, Marcus G., Hamant, Olivier, Krupinski, Pawel, Uyttewaal, Magalie, Ohno, Carolyn, Jönsson, Henrik, Traas, Jan, & Meyerowitz, Eliot M. 2010. Alignment between PIN1 Polarity and Microtubule Orientation in the Shoot Apical Meristem Reveals a Tight Coupling between Morphogenesis and Auxin Transport. *PLoS Biology*, **8**(10), 1–12.

Jönsson, Henrik, Heisler, Marcus G., Shapiro, Bruce E., Meyerowitz, Elliot M., & Mjolsness, Eric. 2006. An auxin-driven polarized transport model for phyllotaxis. *Proceedings of the National Academy of Sciences*, **103**(5), 1633–1638.

Kramer, Eric M. 2002. A Mathematical Model of Pattern Formation in the Vascular Cambium of Trees. *Journal of Theoretical Biology*, **216**, 147–158.

Kramer, Eric M., & Groves, Joseph V. 2003. Defect coarsening in a biological system: The vascular cambium of cottonwood trees. *Physical Review E*, **67**, 041914.

Maynard Smith, John. 1982. *Evolution and the Theory of Games.* Cambridge University Press.

Merks, Roeland M.H., Van de Peer, Yves, Inzé, Dirk, & Beemster, Gerrit T.S. 2007. Canalization without flux sensors: a traveling-wave hypothesis. *TRENDS in Plant Science*, **12**(9), 384–390.

Merks, Roeland M.H., Guravage, Michael, Inzé, Dirk, & Beemster, Gerrit T.S. 2011. VirtualLeaf: An Open-Source Framework for Cell-Based Modeling of Plant Tissue Growth and Development. *Plant Physiology*, **155**(February), 656–666.

Michaelis, L., & Menten, M.L. 1913. Die Kinetik der Invertinwirkung. *Biochemische Zeitschrift*, **49**, 333–369.

Mitchison, G.J. 1981. The Effect of Intracellular Geometry on Auxin Transport II. Geotropism in Shoots. *Proceedings of the Royal Society of London*, **B 214**, 69–83.

Noble, Denis. 2006. *The Music of Life: Biology Beyond Genes.* Oxford University Press.

Raven, Peter H., Evert, Ray F., & Eichhorn, Susan E. 1999. *Biology of Plants*. 6th edn. W.H. Freeman and Company/Worth Publishers.

Smith, Richard S., Guyomarc'H, Soazig, Mandel, Therese, Reinhardt, Didier, Kuhlemeier, Cris, & Prusinkiewicz, Przemyslaw. 2006. A plausible model of phyllotaxis. *Proceedings of the National Academy of Sciences*, **103**(5), 1301–1306.

Turing, A.M. 1952. The Chemical Basis of Morphogenesis. *Philosphical Transactions of the Royal Society*, **B 237**, 37–72.

Yoshida, Saiko, Barbier de Reuille, Pierre, Lane, Brendan, Bassel, George W., Prusinkiewicz, Przemyslaw, Smith, Richard S., & Weijers, Dolf. 2014. Genetic Control of Plant Development by Overriding a Geometric Division Rule. *Developmental Cell*, **29**(April), 75–87.

Zaban, Beatrix, Liu, Wenwen, Jian, Xingyu, & Nick, Peter. 2014. Plant Cells Use Auxin Efflux to Explore Geometry. *Scientific Reports*, **4**(5852), 1–8.